

A pronounced decline in northern vegetation resistance to flash droughts from 2001 to 2022

Received: 9 May 2024

Accepted: 13 March 2025

Published online: 27 March 2025

Miao Zhang^{1,2,3,4}, Xing Yuan^{1,2,3} , Zhenzhong Zeng^{5,6}, Ming Pan⁷,
Peili Wu⁸, Jingfeng Xiao⁹ & Trevor F. Keenan¹⁰ 

Climate change has led to the transition of droughts into rapid and intensified phenomena known as flash droughts, presenting considerable challenges for risk management, particularly concerning their impact on ecosystem productivity. Quantifying the ecosystem's capacity to maintain productivity during flash droughts, referred to as ecosystem resistance, is crucial to assess drought impacts. However, it remains uncertain how the resistance of ecosystem productivity to flash drought changes over time. Here we show that vegetation resistance to flash droughts declines by up to 27% ($\pm 5\%$) over the Northern Hemisphere hotspots during 2001–2022, including eastern Asia, western North America, and northern Europe. The notable decline in vegetation resistance is mainly attributed to increased vapour pressure deficit and temperature, and enhanced vegetation structural sensitivity to water availability. Flash droughts pose higher ecological risks than slowly-developing droughts during the growing seasons, where ecosystem productivity experiences faster decline rates with a shorter response time. Our results underscore the limited ecosystem capacity to resist flash droughts under climate change.

Droughts are becoming more frequent and intense, with a rapid onset under climate change^{1–5}. Among them, flash droughts have attracted substantial attention recently due to their sudden and devastating impacts on numerous regions worldwide, occurring without sufficient early warnings^{5,6}. For instance, a flash drought in 2012 swept over the U.S. Great Plains during a two-month period, significantly impacting agricultural productivity and the carbon sink^{7,8}. The outsized flash drought impacts are exacerbated by accumulated precipitation deficits in conjunction with elevated evaporative demand resulting from increased temperatures^{5,9–11}. Despite their relatively short duration at

the sub-seasonal scale, flash droughts exert rapid stress on ecosystem productivity due to the compound impact of abnormal hydro-meteorological conditions. They impair vegetation physiological functions, including stomatal conductance and biochemical processes^{12–14}, as well as vegetation structure¹⁵. Flash droughts have become more frequent in recent decades under a warming climate, with a higher rate of drought intensification^{5,16–18}. However, the capacity of vegetation to resist flash droughts remain largely unexplored and the global hotspots at risk remain largely unidentified, both of which are essential for effective drought risk assessment and management.

¹School of Hydrology and Water Resources, Nanjing University of Information Science and Technology, Nanjing, China. ²State Key Laboratory of Earth System Numerical Modeling and Application, Institute of Atmospheric Physics, Chinese Academy of Sciences, Beijing, China. ³Key Laboratory of Hydro-meteorological Disaster Mechanism and Warning of Ministry of Water Resources, Nanjing University of Information Science and Technology, Nanjing, China. ⁴Department of Environmental Science, Policy and Management, University of California, Berkeley, USA. ⁵School of Environmental Science and Engineering, Southern University of Science and Technology, Shenzhen, China. ⁶Ningbo Institute of Digital Twin, Eastern Institute for Advanced Study, Ningbo, China. ⁷Center for Western Weather and Water Extremes, Scripps Institution of Oceanography, University of California, San Diego, USA. ⁸Met Office Hadley Centre, Exeter, UK. ⁹Earth Systems Research Center, Institute for the Study of Earth, Oceans, and Space, University of New Hampshire, Durham, USA. ¹⁰Climate and Ecosystem Sciences Division, Lawrence Berkeley National Laboratory, Berkeley, USA. ✉e-mail: xyuan2@mail.iap.ac.cn

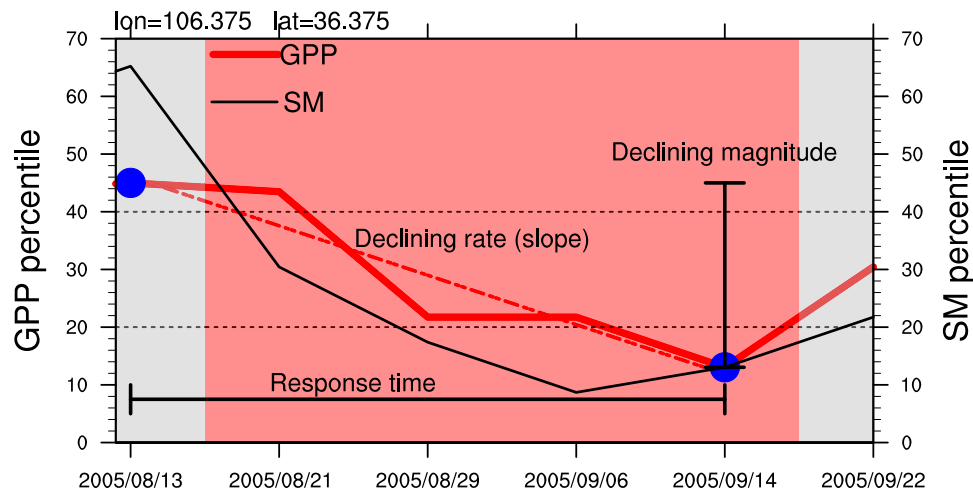


Fig. 1 | An example of the response of ecosystem productivity to sub-seasonal drought. The minimum value of GPP percentiles during the drought period is considered the response intensity of GPP to flash and slow droughts. Response time is the duration of GPP from 8 days before flash droughts to the timing of the occurrence of the minimum GPP value. The loss in GPP

percentiles is defined as the decrease in GPP from 8 days before the onset of droughts to the timing of the minimum values during the drought. Declining rates are calculated as the slopes between the decline in GPP percentiles and response time to represent the resistance of vegetation growth to droughts.

Severe droughts critically impair ecosystem stability and diminish terrestrial gross primary productivity (GPP)^{19–23}. The responses of vegetation to droughts vary across biomes and climates in terms of response times and the severity of the reduction of GPP^{24–27}. The response time refers to the period from the initial undisturbed vegetation condition to the point where vegetation growth is inhibited by droughts, and a longer response time indicates a greater capacity of the ecosystem to withstand water deficits^{13,28}. The magnitude of GPP declines during droughts also reflects the ecosystem drought sensitivity^{21,26,29}. Vegetation resistance to droughts is modulated by concurrent hydrometeorological factors^{30,31}, drought characteristics³², vegetation phenology³³, and vegetation structural and physiological responses³⁴. The dominant factor of carbon losses during droughts is assumed to be soil moisture deficit^{20,35}, while the limitation of vapor pressure deficit (VPD) has become more evident in recent years^{30,36}. Plants can enhance water use efficiency (WUE) to adapt to water stress by closing stomata to limit the water loss through evaporation, albeit at the expense of terrestrial carbon uptake^{37,38}. Recent research^{25,39,40} has documented a widespread decline in ecosystem stability to various environmental perturbations, including droughts, heatwaves, and wildfires, since the early 2000s. Despite these findings, there remains a notable gap in our understanding of how ecosystem resistance specifically to flash droughts varies in the context of ongoing climate change apart from other external disturbances' influence. This knowledge gap hinders our ability to accurately predict terrestrial carbon dynamics under water stress at sub-seasonal scales.

Here we show a pronounced decline in ecosystem productivity resistance to flash droughts across northern hotspots from 2001 to 2022. We utilized a satellite-derived proxy for ecosystem GPP to investigate space-time variations in vegetation resistance to flash droughts on a global scale. We identified all sub-seasonal droughts using multiple soil moisture datasets from ERA5, GLDASv2.1, and GLEAMv3.8a during the growing seasons of 2001–2022. Subsequently, we classified these droughts into two categories, namely flash and slow droughts, based on the rates of soil moisture dry-down in percentiles during the onset stage (Methods and Fig. 1). Two independent satellite records including GPP from Moderate Resolution Imaging Spectroradiometer (MODIS) and sun-induced chlorophyll fluorescence (SIF) derived from the Orbiting Carbon Observatory-2 (OCO-2), were employed. Specifically, we adopted the declining rates in GPP or SIF percentiles to measure ecosystem resistance to droughts, integrating

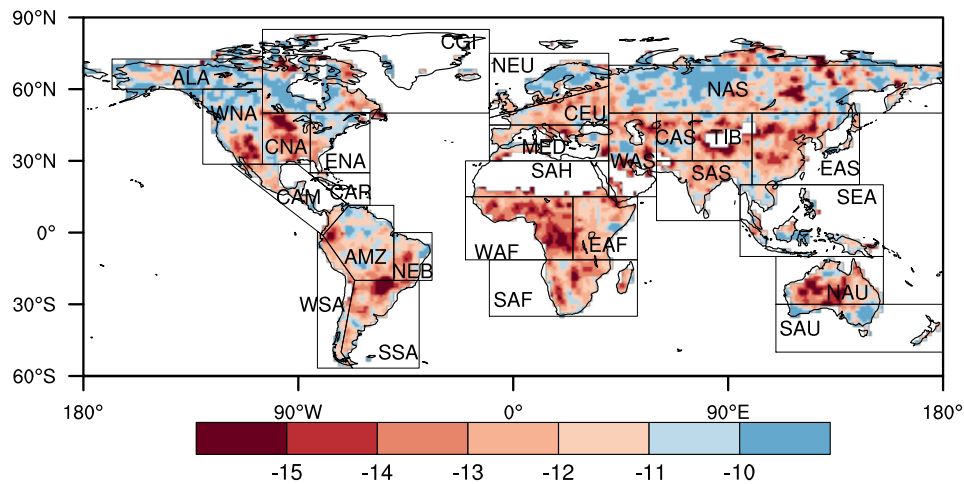
both the response time and declining magnitudes of ecosystem productivity. We examined the global spatial distributions and temporal trends of GPP resistance to flash droughts. To elucidate the observed trends, we employed a random forest model to attribute them to the hydrometeorological anomalies, drought characteristics, and vegetation responses (more details refer to Methods).

Global ecosystem productivity resistance to flash droughts

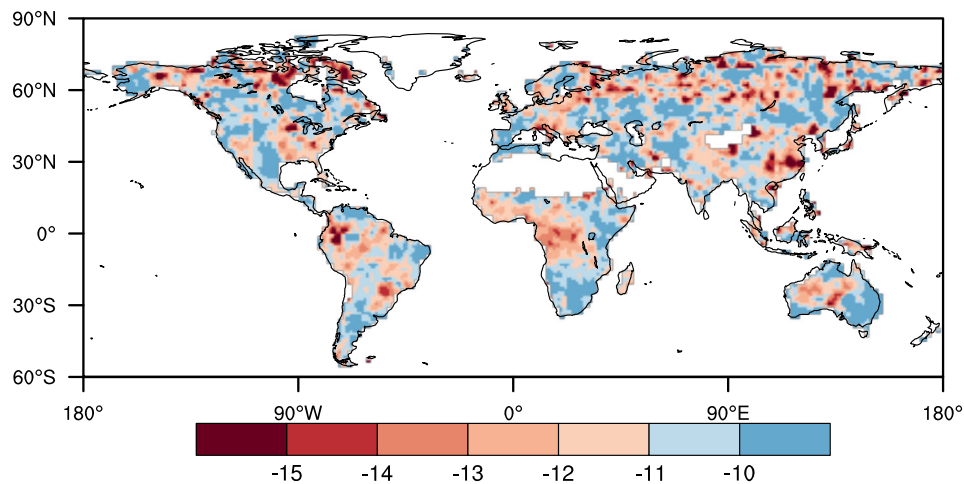
Flash droughts are more likely to occur over eastern, southern, and northern Asia, eastern America, northern Europe, and the Amazon compared to slow droughts (Supplementary Fig. 1). Based on the identified flash and slow drought events at each pixel, we estimated GPP's response time, declining magnitudes, and declining rates to both types of droughts using MODIS-derived GPP and OCO-2 derived SIF (Fig. 1) comparing the undisturbed conditions to the response intensity of GPP (Supplementary Fig. 2). Here, these response proxies represent the ecosystem's capacity to withstand drought disturbances, and the larger GPP decline rate during droughts indicates that the ecosystem's photosynthetic process is less resistant to water stress.

For all flash droughts, the resistance of GPP is quantified by the change rates of GPP percentiles and the global mean resistance is $-12 \pm 0.4\%$ (mean \pm s. d.) per 8 days during the GPP's response period (Fig. 2a). The declining rates are generally larger during flash droughts than slow droughts over 66% of the global vegetated areas (Fig. 2b, c). However, in high latitude regions, the Amazon, and southeastern Asia, the decline in photosynthetic rates under flash droughts is slower than slow droughts. As these regions are energy-limited, the higher temperature and shortwave radiation can offset the negative impacts of droughts^{27,41}. Faster declining rates in GPP are related to the faster response time, with the response time of GPP to flash droughts being only 34 ± 0.1 days from the unperturbed state to the maximum intensity of GPP response, which is shorter than the 39 ± 0.7 days for slow droughts at the significance level of 1% (Supplementary Fig. 3). For the low-latitude and mid-latitude regions except for Amazon and southeastern Asia, the rapid drought intensification of flash droughts imposes compound stress from both soil moisture drought deficit and atmospheric dryness on vegetation growth, driving faster response of GPP. Through comparing the hydrometeorological conditions during flash and slow drought periods, we observed that both soil moisture deficit and atmospheric dryness are more severe during flash droughts

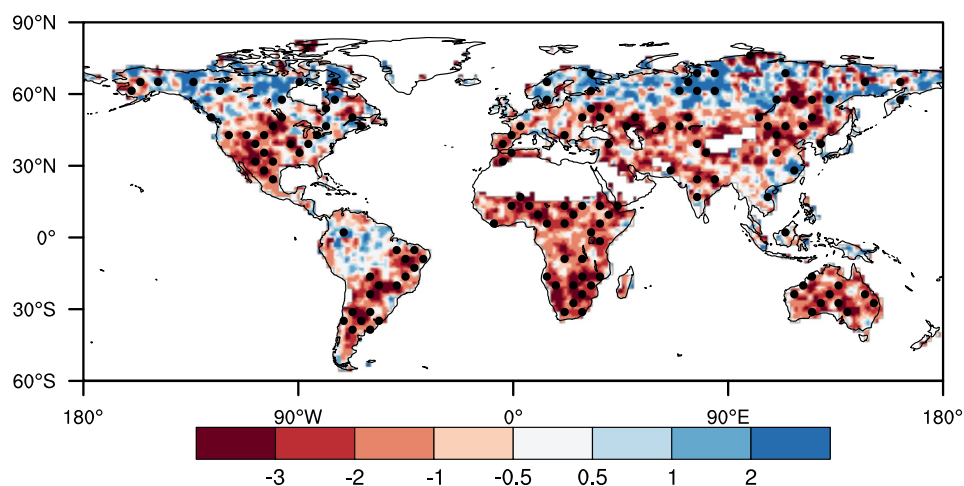
(a) Resistance to flash drought



(b) Resistance to slow drought



(c) Difference between flash drought and slow drought



than slow droughts (Supplementary Fig. 4), resulting in more pronounced limitation on vegetation photosynthesis during flash droughts.

Furthermore, the differences between resistance to flash and slow droughts are larger in drier climate regions, with drylands exhibiting higher vegetation sensitivity to flash droughts

(Supplementary Fig. 5). In terms of different ecosystem types, GPP of all land cover types except for deciduous needleleaf forests shows larger declining rates during flash droughts than those during slow droughts, as the growth of deciduous needleleaf forests in a relatively cold climate are influenced by temperature and radiation (Supplementary Fig. 6).

Fig. 2 | Spatial distributions of vegetation productivity resistance to flash and slow droughts. **a** Global resistance of the terrestrial gross primary productivity (GPP) to flash droughts averaged over 2001–2022. Here, the resistance of GPP is defined as the change rate of GPP percentiles from undisturbed conditions 8 days before the onset of flash drought to the minimum GPP percentiles during the whole drought period. The smaller values indicate less resistance of vegetation to droughts (see Methods for details). **b** The same as (a), but for GPP resistance to slow droughts. **c** The

differences between GPP resistance to flash droughts and slow droughts. Black spots represent differences that pass the two-sided significance test of the Student's *t* test with a *P*-value < 0.05. Here the gridded resistance index is averaged over all flash and slow drought events from six ensemble members based on three soil moisture products including ERA5, GLDASv2.1, and GLEAMv3.8a, and two vegetation productivity products including MODIS-derived GPP and solar-induced chlorophyll fluorescence (SIF). The values for raw 0.25-degree grids are clustered into $2^\circ \times 2^\circ$ moving windows.

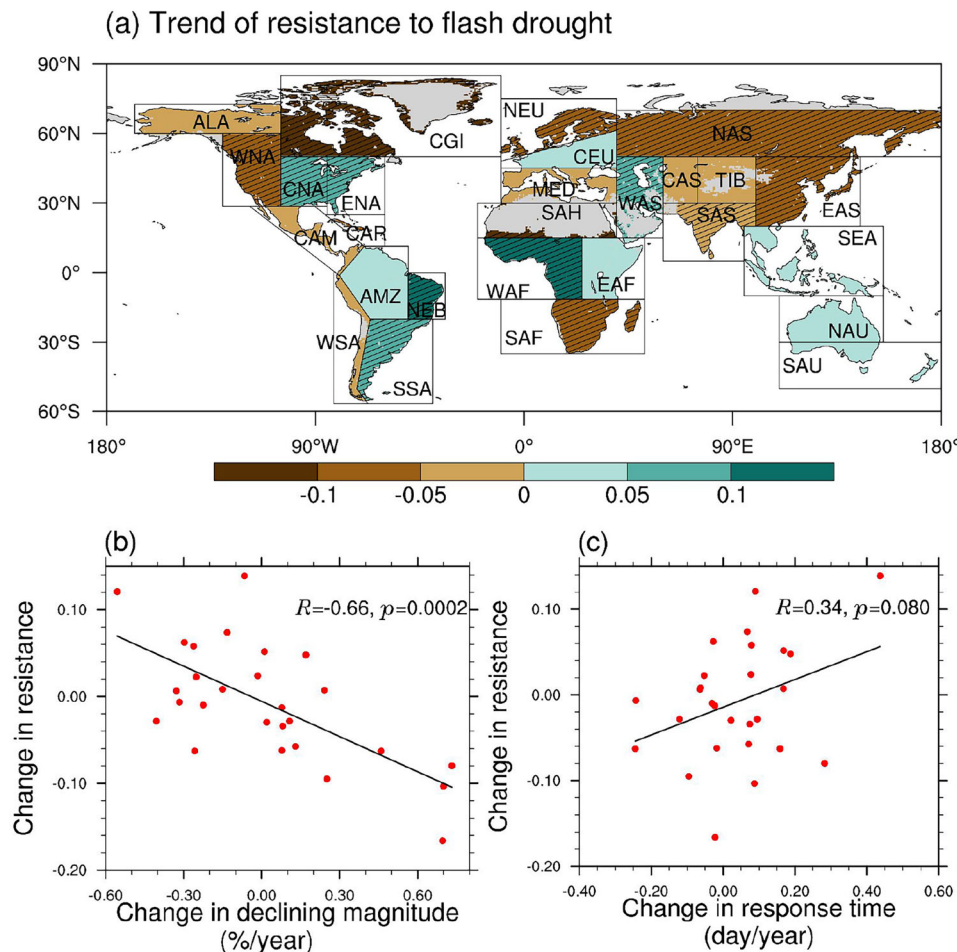


Fig. 3 | Regional trends in vegetation productivity resistance to flash droughts during 2001–2022 and their associations with decline magnitude and response time of vegetation productivity. **a** The linear trends of 5-point running average resistance to flash droughts over the 27 IPCC SREX regions. Brown and turquoise color polygons indicate declining and increasing trends in the ensemble of vegetation resistance to flash droughts derived from multiple datasets, respectively, and the regions with black hatchings indicate the trend is significant with a 95% confidence level. **b, c** Relationship between trends of

resistance and declining magnitudes ($\% \text{ yr}^{-1}$)/response time (days yr^{-1}) of GPP for the IPCC SREX regions. Declining magnitudes are quantified as the percentage ratio of the difference between the minimum GPP and GPP values during 8 days before flash droughts (GPPpre) to GPPpre. Response time is the lag between the time of the minimum GPP values and the onset timing of flash droughts. *R* represents the Pearson linear correlation coefficient between trends in response magnitude/response time and resistance, assessed using a two-sided Student's *t* test.

Trend of ecosystem productivity resistance to flash droughts

To investigate the regional changes in the vegetation productivity resistance to flash droughts, the gridded declining rates were averaged over 27 IPCC SREX regions weighted by grid areas. We find that GPP declining rates over the flash drought periods increased by $6 \pm 4\%$ – $27 \pm 5\%$ in eastern, southern, and northern Asia, northern Europe, western North America, southern Africa, Sahara, and Canada region during 2001–2022 (Fig. 3a and Supplementary Fig. 7). Notably, the significant declines ($p < 0.01$) in GPP resistance to flash droughts are $16 \pm 3\%$, $12 \pm 1\%$ and $12 \pm 6\%$ over eastern Asia, West North America, and North Europe during 2001–2022. The vegetation in northern regions is increasingly sensitive to flash droughts, with 34% of

vegetated land across the Northern Hemisphere exhibiting accelerated declining rates in GPP during flash droughts (Fig. 3a). Instead, the resistance of vegetation over Central North America, East North America, Southeast South America, North-East Brazil, West Africa, and West Asia is increasing during recent two decades (Fig. 3a and Supplementary Fig. 8). Although the resistance trends vary across different regions based on various soil moisture products, there is a high consistency in the trends' direction across individual results such as eastern Asia, southern Africa, West Africa, and southern South America (Supplementary Fig. 9). Generally, vegetation photosynthesis demonstrates greater sensitivity to flash droughts over most Northern Hemisphere regions ($p = 0.30$), whereas it exhibits more resistance over the Southern Hemisphere ($p < 0.01$).

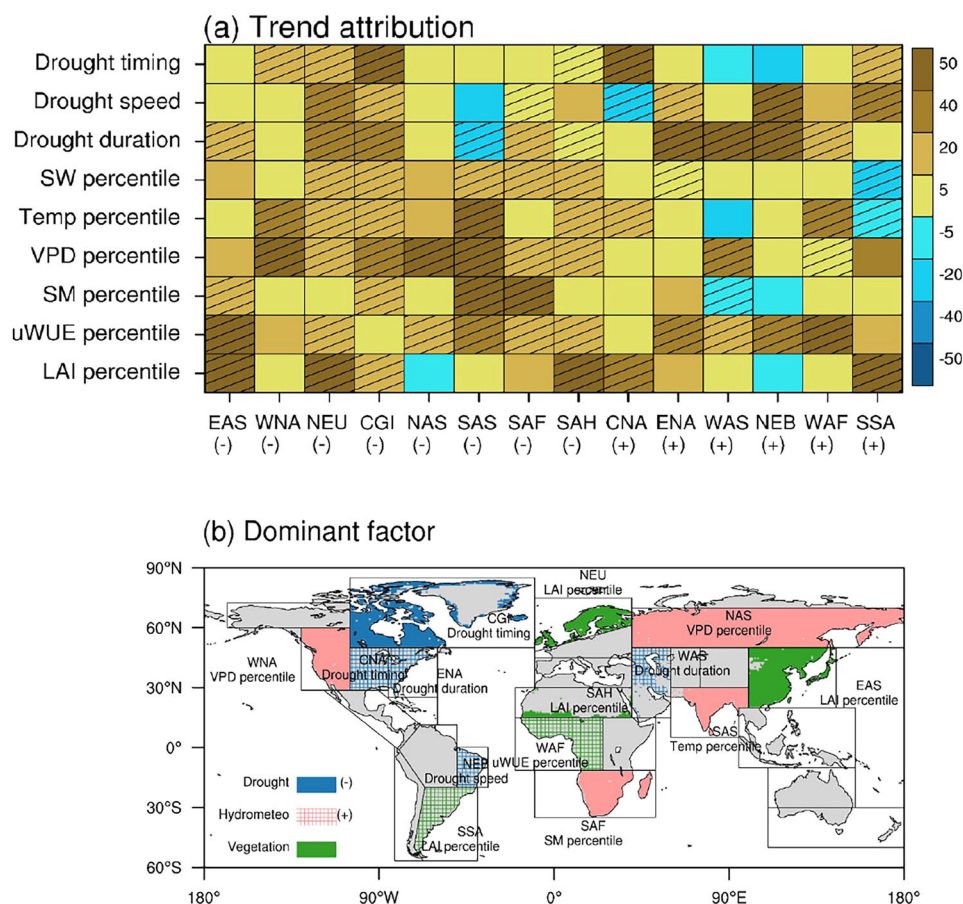


Fig. 4 | Potential drivers of temporal changes in GPP resistance to flash droughts. **a** The contribution (%) of each factor to the decreasing/increasing GPP resistance. Nine factors from three categories including drought characteristics (drought timing, drought speed, and drought duration), hydrometeorological conditions during flash droughts (percentiles of shortwave radiation (SW), temperature (Temp), vapor pressure deficit (VPD), and soil moisture (SM) during flash droughts), and vegetation response (leaf area index (LAI) and underlying water use efficiency (uWUE) to flash droughts) were selected to quantify their contributions.

Positive values of a certain variable mean that the variable contributes positively to the changes in resistance. **b** The dominant drivers over the eight regions (CGI, NEU, NAS, WNA, EAS, SAH, SAS, and SAF) with significant declining GPP resistance and six regions including CNA, ENA, WAS, NEB, SSA, and WAF with increasing resistance. Polygons in blue, pink, and green represent that the dominant roles in driving the changes in regional resistance are the changing drought characteristics, hydrometeorological conditions, and vegetation response, respectively.

We analyzed the relationship between the temporal changes in resistance indicated by the rates and magnitudes/response time of GPP decline for the period 2001–2022 over the IPCC SREX regions during flash droughts (Fig. 3b, c). The temporal changes in resistance are negatively correlated with those in declining magnitudes, with a correlation coefficient of -0.66 ($p = 0.0002$), and positively correlated with response time ($r = 0.34$, $p = 0.080$). This suggests that the higher declining rates in GPP during flash droughts are more influenced by the loss of vegetation photosynthesis (magnitude) than by the response time. This observation aligns with previous studies^{21,42} asserting that drought is increasingly influential on ecosystem carbon uptake, and the drought-induced reduction of GPP is on the rise.

Potential drivers of the declining flash drought resistance

To delve into the contribution of plant traits and environmental factors to the changes in vegetation resistance during flash droughts, we applied the random forest regression model⁴³, a machine learning method, to relate GPP's declining rates during the drought period to drought characteristics, hydrometeorological conditions, and vegetation responses. Here nine predictors were used to regress GPP resistance to flash droughts at an annual time step through the random forest model, and the trends of modeled resistance were consistent

with the observed trends (Supplementary Fig. 10). Subsequently, we conducted a focused analysis on the influence of the temporal changes of different factors on vegetation resistance to flash droughts.

For eastern Asia, the reduction in percentiles of detrended LAI during flash droughts is increasingly severe ($p = 0.02$), and the increasing LAI sensitivity to flash droughts contributes to the most ($53 \pm 17\%$) of the declining trend in resistance (Fig. 4a and Supplementary Fig. 11a). In addition, the declining LAI under water stress also contribute most to the declining resistance over northern Europe and Sahara (Supplementary Fig. 11c, h). Whereas vegetation growth benefits from warming, CO_2 fertilization effects, and forest conservation policy^{44,45}, the enhanced vegetation growth can further deplete soil moisture and may be beyond the ecosystem capacity and intensify climate extremes' ecological impacts on vegetation structure^{46,47}. For West North America, North Asia, and South Asia, the increase in percentiles of VPD and temperature contributes most to the decreased resistance to flash droughts ($46 \pm 6\%$ – $96 \pm 9\%$; Fig. 4b and Supplementary Fig. 11b, e, f). For southern Africa, the drying soil moisture explains $54 \pm 7\%$ of the declining resistance (Supplementary Fig. 11g). The flash drought enhances land-atmosphere interactions, further intensifying water stress on vegetation physiological process and decreasing the stomatal conductance. The onset of flash drought over northeastern Canada becomes earlier before the peak of the growing

season (Supplementary Fig. 11d), contributing $56 \pm 4\%$ to the temporal changes in resistance. The dominant role in driving faster response of GPP varies across different regions. The decrease in resistance observed in 50% of the regions (4 out of 8 regions) is related to increasing VPD and temperature and decreasing soil moisture. However, there are still large variations of vegetation sensitivity to flash droughts that cannot be explained by the random forest model.

For the increased resistance in certain regions, the delayed drought onset after the peak of the growing season, the increased drought duration, and decreased drought speed, or the increased underlying water use efficiency (uWUE) and decreased LAI sensitivity to droughts played an important role (Fig. 4b and Supplementary Fig. 12), optimizing carbon fixation while minimizing water loss and offsetting negative impacts of droughts on the carbon sink. In addition, longer drought duration prolongs the duration of GPP response, thereby mitigating the decline in GPP rates.

Discussion

Our combined use of satellite observations, reanalysis hydro-meteorological data, and a machine learning model suggests that the accelerated GPP decline during flash droughts in recent decades presents challenges for unraveling the mechanism of climate change impacts and monitoring vegetation health and assessing drought-related risks, especially for agricultural regions (e.g., eastern Asia, southern Asia, and western North America). Our results reveal the rapid decline rates in terrestrial ecosystems' productivity under short-term intensified droughts, especially in the water-limited regions, which were overlooked by previous studies^{21,48}. The concurrent extreme atmospheric dryness and soil moisture deficits during flash droughts, resulting in reduced resistance of plants to these abrupt events. This sharper decline in ecosystem productivity during flash droughts, coupled with shorter recovery intervals due to their increasing frequency^{5,49}, underscores the growing threat they pose to ecosystem stability. Future research efforts should delve into how vegetation recovers from flash droughts, as post-drought recovery is pivotal in assessing the ecosystem resilience to droughts⁵⁰.

Notably, our results highlight that 37% of the vegetated land over the Northern Hemisphere shows significant decreasing resistance to flash droughts, warning that vegetation resistance to flash droughts in northern regions is probably limited under growing climate change. Various factors during flash droughts are undermining different capacities for drought resistance simultaneously. Our results emphasize that extreme hydrometeorological conditions weaken the terrestrial ecosystem's ability to withstand flash droughts under climate change, dominating the declining trends in resistance in over 50% of hotspot regions, with their contributions ranging from $46 \pm 6\%$ to $96 \pm 9\%$. Vegetation structural overshoot, where warming results to temporary increases in the vegetation carrying capacity is expected to further exacerbate the sensitivity of vegetation to soil moisture declines⁴⁶. However, limitations must be considered when interpreting these changes in resistance. The coarse coverage of resistance at a regional scale could overlook variations across a wide range of climates and terrestrial ecosystems. Therefore, long-term terrestrial ecosystem productivity datasets at finer spatio-temporal scales based on advancements in remote sensing techniques, earth system models, and deep learning algorithms are urgently needed to facilitate more detailed studies.

The increasing concurrence of soil moisture deficits and atmospheric dryness exacerbates the flash drought risk in a warming climate⁵. The interactions between vegetation and the water cycle are increasingly intertwined and plant hydraulic and photosynthetic processes would become more vulnerable under compound water stresses, particularly in high-emission scenarios⁵¹. This research highlights the growing vulnerability of ecosystem productivity to flash droughts as climate warms. A better understanding of anthropogenic climate

change's influence on vegetation responses to flash droughts will inform adaptive strategies and interventions to safeguard ecosystem health and resilience in the face of climate change. Furthermore, with the aim of achieving a carbon neutrality target, further investigations of the mechanisms behind flash droughts and their impact on ecosystem productivity contribute to the improvement of modeling and predicting dynamics of the carbon cycle in the future.

The observed declining resistance to flash droughts in our study underscores the urgent need for enhanced monitoring and management strategies to mitigate the adverse impacts of flash droughts on terrestrial ecosystems. More frequent flash droughts threaten global food security, particularly when occurring during the critical period of crop growth^{52–54}. Therefore, skillful and reliable flash drought impact forecasts on subseasonal-to-seasonal timescales are increasingly critical for flash drought preparation and mitigation^{25,55}. The timely effective information for impending flash drought events can form the basis for reducing the vulnerability of natural and agricultural systems at risk⁸.

Methods

Hydrometeorological data

Three global reanalysis soil moisture datasets were used to identify flash and slow drought events including ECMWF Reanalysis v5 (ERA5)⁵⁶, The Global Land Data Assimilation System version 2.1 (GLDASv2.1)⁵⁷, and Global Land Evaporation Amsterdam Model version 3.8a (GLEAM3.8a)⁵⁸. For ERA5 and GLDASv2.1, the soil moisture data were interpolated into from ground surface down to 1-m. For GLEAMv3.8a, the root-zone soil moisture was used. Considering there is a large uncertainty of soil moisture estimates, here the ensemble mean results based on these three datasets were used^{59,60}. The meteorological conditions during the drought period were also examined, including precipitation (P), potential evapotranspiration (PET), air temperature (Temp), VPD, evapotranspiration (ET), and shortwave radiation (SW) mainly from ERA5. In this study, we processed the hydrometeorological variables from hourly or daily raw data into 8-day timescale to be consistent with the temporal intervals of satellite ecosystem productivity data. The calculation of uWUE ($\frac{GPP \cdot \sqrt{VPD}}{ET}$)⁶¹ used corresponding evapotranspiration that was consistent with the corresponding soil moisture data used. The climate classification was based on multiyear mean aridity index ($AI = P/PET$), and climate regions included hyper-arid ($AI < 0.05$), arid ($0.05 \leq AI < 0.2$), semi-arid ($0.2 \leq AI < 0.5$), dry sub-humid ($0.5 \leq AI < 0.65$), and humid regions ($0.65 \leq AI$)⁶².

Remote sensing data

Here two independent satellite proxies were used to examine the ecosystem productivity's response to droughts during the period from 2001 to 2022, including MODIS-derived GPP and SIF from the global OCO-2 SIF product (GOSIF). GPP from MODIS was estimated based on the light-use efficiency model which was formulated as the product of the incident photosynthetically active radiation (PAR), the fraction of absorbed PAR, and the light-use efficiency⁶³, and missing observations were filled by using the linear interpolation method. SIF is considered a major advancement in measuring terrestrial photosynthesis, and it shows a strong relationship with GPP^{64,65}. Specifically, SIF shows earlier responses to drought than traditional vegetation indexes⁶⁶. Here we used the GOSIF dataset, which was produced using a data-driven approach based on OCO2-SIF, remote sensing data from MODIS, and meteorological reanalysis data⁶⁷. We also analyzed the changes in vegetation structure during droughts using LAI from Global Land Surface Satellite (GLASS) MODIS LAI products. The land cover classification is based on MODIS. All datasets were interpolated into 0.25° spatial resolution.

Flash drought identification

Soil moisture acts as the indicator of flash droughts, as the dynamics of soil moisture are typically associated with lower precipitation and

humidity and increased solar radiation and temperature^{6,68} and are closely related to vegetation water stress^{13,34}. The definition of flash and slow droughts refers to Yuan et al.⁵. Firstly, the soil moisture data were aggregated into the 8-day time scale at each pixel (e.g., Jan 1st to Jan 8th) to be consistent with satellite observation frequency, and were then transformed into percentiles by ranking them at each 8-day time step from 2001 to 2022. The sub-seasonal droughts start from the soil moisture percentiles below 40% and develop into the minimum values below 20%. Once the soil moisture percentiles recover above the threshold of 20%, the droughts end. To remove events with little ecological influence, the total duration should be no shorter than 4 time steps (i.e., 32 days), and there should be at least three 8-day time steps with soil moisture percentiles below 20%⁶⁹. Besides, mean anomalies of ET should be negative (ET percentile <50%) during the drought period, indicating water stresses on vegetation, although higher atmospheric demand may drive more ET during the onset stage of droughts. The identified sub-seasonal droughts were further classified into flash and slow droughts based on the declining rates of soil moisture percentiles. For flash droughts, the average declining rate of soil moisture percentiles during the onset stage is no less than 5% per 8 days, otherwise, they are classified as slow droughts. Based on this definition, the ratio of flash drought events with declining GPP is 99% and this method allows a reasonable quantification of the negative impacts of flash droughts through the constraint of mean ET percentiles <50% and the duration at least lasting for 32 days.

The characteristics of flash droughts were used to investigate the relationship between flash drought and vegetation productivity resistance, including duration, speed of soil moisture intensification, and the timing of drought onset. According to Yuan et al.⁵, the duration of flash drought was determined as the persistence time starting from the soil moisture below 40th percentile to below 20th percentile, and recovers above the 20th percentile. The onset speed of flash drought was determined as the declining rates in soil moisture percentiles from a relatively normal condition of 40% to the lowest soil moisture percentile during flash drought. Considering the droughts' impact on vegetation, here we only focused on the growing seasons identified by the multiyear-averaged LAI at an 8-day time scale. If the LAI peak of the growing season lies between April to September, the growing cycle starts from January and ends in December, otherwise, the growing cycle starts from the previous May to the current April. The start and end of the growing season are the points of the minimum LAI in the annual cycle plus 25% of the amplitude between the maximum and minimum values⁷⁰. If the minimum LAI is greater than 2, the growing season at this grid is considered as a whole year, as the vegetation exists throughout the whole year. The length of the growing seasons is shown in Supplementary Fig. 13.

In this study, we excluded those sub-seasonal drought events if the GPP percentile is below 40% before the onset of droughts, as these cases are difficult to disentangle the influence of droughts on vegetation growth from other external disturbances.

Response of ecosystem productivity to flash droughts

Before analyzing the ecosystem response to droughts, GPP was detrended at each time step in the annual cycle and transformed into percentiles to remove the seasonal effect and long-term trend⁴⁰. The response of GPP to flash droughts (or slow droughts) is measured using response time, declining magnitudes, and the rate of GPP decline during the drought period (Fig. 1). For each drought event at a 0.25° grid, first, we determined the timing of the occurrence of the minimum value of GPP percentiles during the drought period, thus the response time of GPP spans from 8 days before flash droughts under normal conditions (GPP percentiles >40%; Supplementary Fig. 2a), to the timing of the minimum GPP percentiles (Supplementary Fig. 2b)^{13,24}. We then calculated the difference between GPP conditions during

8 days before flash droughts and the minimum GPP percentiles to quantify the declining magnitude²¹. The slope between the response time and declining magnitude during the response period reflects the sensitivity of GPP to flash droughts (or slow droughts)²⁶, and the larger slopes (larger magnitudes of negative values) indicate the less resistance of GPP to flash or slow droughts.

To verify the reliability of remote sensing-derived vegetation productivity, we used in-situ observations of GPP at 80 eddy covariance towers where flash droughts/slow droughts occurred during the study period. These observations were derived from FLUXNET 2015, AmeriFlux FLUXNET, ICOS Warm Winter 2020, OzFlux, and ChinaFLUX (Supplementary Tab. 1). Although there is a large mismatch in spatial scales between the tower footprint (typically with diameters of a few hundred meters) and the 0.25-degree grid cells, satellite-derived resistance and response time show significant correlations with in-situ results, with correlation coefficients (*R*) of 0.21/0.29 (MODIS-GPP/SIF with *p* < 0.001/0.002) and 0.33/0.45 (MODIS-GPP/SIF with *p* < 0.001), respectively.

Here three sets of flash and slow drought events were identified using three soil moisture products as mentioned above, and then the response of vegetation productivity to the identified drought events was individually detected using two vegetation productivity products including MODIS-derived GPP and SIF. The temporal dynamics of resistance were analyzed by linear trends and then a two-sided *t*-test was applied for the individual linear trend derived from six members. The ensemble mean of the six members was used for climatology and trend analysis, and the uncertainty was quantified by the standard deviation through 1000 times bootstrap sampling with the replacement of members^{60,71}.

Attribution of resistance trends

We applied the random forest model⁴³ to investigate a set of potential drivers of the changes in vegetation resistance to flash droughts, including the vegetation physiological and structural responses indicated by uWUE and LAI, and environmental factors including the soil moisture (SM), Temp, VPD, SW, and drought characteristics (e.g., duration, speed, and onset timing). The percentiles of hydrometeorological variables including SM, Temp, VPD, and SW during the drought period were used to represent the intensity of perturbations, respectively. The drought timing is quantified as the difference between the onset of drought and the peak of LAI in the annual cycle. The negative values of drought timing indicate that droughts start before the peak of the growing season, and vice versa. The random forest model was developed using the regional average GPP resistance to flash drought and the regional mean drought characteristics, hydrometeorological conditions, and vegetation responses averaged during flash drought events over each grid within the region at an annual time step. We found that the model explained 80–96% of the variations of vegetation resistance across sites and the modeled resistance also showed the same direction of trends with the observed results (Supplementary Fig. 10). Compared with the multiple linear regression model (*R*² = 0.36), the random forest model has a better performance in the simulation of resistance (*R*² = 0.88), by considering the nonlinear interactions between influencing factors and resistance, without a priori assumption about the functional form. Furthermore, we applied the random forest model to disentangle the temporal changes in resistance due to the variations of different factors. To quantify the marginal contributions of each predictor, the control experiment accounted for the dynamics of all predictors, whereas the sensitivity experiment considered all predictors' dynamics except for the target predictor. The changes in resistance due to the dynamics of a certain factor were disentangled as follows:

$$\Delta Y_a = \Delta f(X^t) - \Delta f(X_{-a}^t, X_a^{t_0}) \quad (1)$$

in which f is the random forest model, and X and Y represent multiple predictors and ecosystem productivity's resistance to flash droughts, respectively. The second term on the right side of Eq. (1) is the random forest model simulation considering all predictors' dynamics except for the predictor of X that was kept constant to a certain year of t_0 and Δ represents the linear trend of the model simulation. Due to the availability of GLASS LAI, the attribution analysis was based on the period of 2001–2021. For the attribution of each predictor to the temporal changes in resistance, the experiments were conducted with one predictor fixed at each year of 2001–2021, respectively. The contribution of each factor to the temporal changes of GPP resistance was calculated by the ratio of the difference between the resistance trend in the factor-fixed and control experiments to the modeled trend in the control experiment. If there are over 90% of the 21 members of the experiments showing the same direction of change of resistance trend influenced by a certain factor, the contribution of the factor was assumed to be significant.

Sensitivity analysis

To assess the robustness of the spatio-temporal characteristics of resistance with respect to the threshold choices in defining flash droughts, we conducted a series of sensitivity analyses by altering the thresholds used in the flash drought definition. Specifically, we changed the start point of flash droughts from soil moisture percentiles above 40 to 50%, to represent a relatively normal pre-drought conditions, and the drought termination from soil moisture percentiles recover above 20% to 10%, to represent the extreme drought category. We also adjusted the minimum drought duration from 4 time steps (32 days) to 3 time steps (24 days) and considered pre-drought ecosystem productivity levels from above 40% to 50% to represent undisturbed vegetation conditions before droughts. Furthermore, we also examined the spatial distributions and temporal trends using different thresholds. While the absolute values of resistance to flash and slow droughts varied with different thresholds, the results show a high overall consistency in the patterns of resistance differences between flash droughts and slow droughts, as shown in Fig. 2c (R : 0.75–0.98, $p < 0.01$). Additionally, 59%–69% of grids exhibited negative differences, indicating that the ecosystem productivity's resistance to flash droughts is generally lower than slow droughts (Supplementary Fig. 14). Furthermore, the results with different thresholds show similar temporal changes in resistance over hotspot regions (Supplementary Fig. 15). Overall, the sensitivity analysis demonstrates that the different thresholds do not affect the spatio-temporal dynamics of ecosystem productivity's resistance to flash droughts. The response time of ecosystem productivity, when GPP percentiles were below 20%, was also faster during flash droughts compared to slow droughts (Supplementary Fig. 16), which is consistent with the faster response time of the minimum GPP percentiles during flash droughts.

Reporting summary

Further information on research design is available in the Nature Portfolio Reporting Summary linked to this article.

Data availability

The hydrometeorological data derived from ERA5 are available at <https://cds.climate.copernicus.eu/cdsapp#!/dataset/reanalysis-era5-single-levels?tab=overview>. The soil moisture and evapotranspiration dataset from GLEAMv3.8a is available through <https://www.gleam.eu/>. And for GLDAS, soil moisture and evapotranspiration data are available to download at <https://disc.gsfc.nasa.gov/datasets?keywords=GLDAS>. The GOSIF is obtained through <https://globalecology.unh.edu/data/GOSIF.html>. MODIS GPP and land cover products are available through <https://modis.gsfc.nasa.gov/data/>. GLASS-MODIS LAI is available at <http://glass-product.bnu.edu.cn/introduction1/LAI.html>. The eddy covariance fluxes are available at <https://fluxnet.org/>. The regional boundaries used in this study are based on the IPCC AR5 regions and available at https://www.ipcc-data.org/guidelines/pages/ar5_regions.html.

<https://fluxnet.org/>. The regional boundaries used in this study are based on the IPCC AR5 regions and available at https://www.ipcc-data.org/guidelines/pages/ar5_regions.html.

Code availability

The code for ecosystem productivity resistance to flash droughts is available at <https://github.com/miaozhang2025/Vegetation-resistance-to-flash-drought> (<https://doi.org/10.5281/zenodo.14880927>).

References

1. Ault, T. R. On the essentials of drought in a changing climate. *Science* **368**, 256–260 (2020).
2. Dai, A. Increasing drought under global warming in observations and models. *Nat. Clim. Chang* **3**, 52–58 (2013).
3. Trenberth, K. E. et al. Global warming and changes in drought. *Nat. Clim. Chang* **4**, 17–22 (2014).
4. Pokhrel, Y. et al. Global terrestrial water storage and drought severity under climate change. *Nat. Clim. Chang* **11**, 226–233 (2021).
5. Yuan, X. et al. A global transition to flash droughts under climate change. *Science* **380**, 187–191 (2023).
6. Otkin, J. A. et al. Flash droughts: A review and assessment of the challenges imposed by rapid-onset droughts in the United States. *Bull. Am. Meteorol. Soc.* **99**, 911–919 (2018).
7. Hoerling, M. E. et al. Causes and predictability of the 2012 great plains drought. *Bull. Am. Meteorol. Soc.* **95**, 269–282 (2014).
8. Pendergrass, A. G. et al. Flash droughts present a new challenge for subseasonal-to-seasonal prediction. *Nat. Clim. Chang* **10**, 191–199 (2020).
9. Zhao, M., A. G., Liu, Y. & Konings, A. G. Evapotranspiration frequently increases during droughts. *Nat. Clim. Chang* **12**, 1024–1030 (2022).
10. Qing, Y., Wang, S., Ancell, B. C. & Yang, Z.-L. Accelerating flash droughts induced by the joint influence of soil moisture depletion and atmospheric aridity. *Nat. Commun.* **13**, 1–10 (2022).
11. Christian, J. I. et al. Global distribution, trends, and drivers of flash drought occurrence. *Nat. Commun.* **12**, 1–11 (2021).
12. Sungmin, O. & Park, S. K. Flash drought drives rapid vegetation stress in arid regions in Europe. *Environmental Research Letters* **18**, (2023).
13. Zhang, M. & Yuan, X. Rapid reduction in ecosystem productivity caused by flash droughts based on decade-long FLUXNET observations. *Hydrol. Earth Syst. Sci.* **24**, 5579–5593 (2020).
14. He, M. et al. Impacts of the 2017 flash drought in the US Northern plains informed by satellite-based evapotranspiration and solar-induced fluorescence. *Environ. Res. Lett.* **14**, 074019 (2019).
15. Zhang, M., Yuan, X. & Otkin, A. J. Remote sensing of the impact of flash drought events on terrestrial carbon dynamics over China. *Carbon Balance Manag.* **15**, 20 (2020).
16. Wang, Y. & Yuan, X. Anthropogenic Speeding Up of South China Flash Droughts as Exemplified by the 2019 Summer-Autumn Transition Season. *Geophys Res. Lett.* **48**, e2020GL091901 (2021).
17. Yuan, X. et al. Anthropogenic shift towards higher risk of flash drought over China. *Nat. Commun.* **10**, 4661 (2019).
18. Mishra, V., Aadhar, S. & Mahto, S. S. Anthropogenic warming and intraseasonal summer monsoon variability amplify the risk of future flash droughts in India. *NPJ Clim. Atmos. Sci.* **4**, 1–10 (2021).
19. Humphrey, V. et al. Soil moisture–atmosphere feedback dominates land carbon uptake variability. *Nature* **592**, 65–69 (2021).
20. Green, J. K. et al. Large influence of soil moisture on long-term terrestrial carbon uptake. *Nature* **565**, 476–479 (2019).
21. Gampe, D. et al. Increasing impact of warm droughts on northern ecosystem productivity over recent decades. *Nat. Clim. Chang* **11**, 772–779 (2021).
22. Xu, C. et al. Increasing impacts of extreme droughts on vegetation productivity under climate change. *Nat. Clim. Chang* **9**, 948 (2019).

23. Piao, S. et al. The impacts of climate extremes on the terrestrial carbon cycle: A review. *Sci. China Earth Sci.* **62**, 1551–1563 (2019).
24. Vicente-Serrano, S. M. et al. Response of vegetation to drought time-scales across global land biomes. *Proc. Natl Acad. Sci. USA* **110**, 52–57 (2013).
25. Li, X. et al. Temporal trade-off between gymnosperm resistance and resilience increases forest sensitivity to extreme drought. *Nat. Ecol. Evol.* **4**, 1075 (2020).
26. Lloret, F., Keeling, E. G. & Sala, A. Components of tree resilience: Effects of successive low-growth episodes in old ponderosa pine forests. *Oikos* **120**, 1909–1920 (2011).
27. Miller, D. L. et al. Increased photosynthesis during spring drought in energy-limited ecosystems. *Nat Commun* **14**, 7828 (2023).
28. Sun, S. et al. Response of Gross Primary Productivity to Drought Time-Scales Across China. *J. Geophys Res Biogeosci* **126**, 1–19 (2021).
29. Von Buttlar, J. et al. Impacts of droughts and extreme-temperature events on gross primary production and ecosystem respiration: A systematic assessment across ecosystems and climate zones. *Biogeosciences* **15**, 1293–1318 (2018).
30. Yuan, W. et al. Increased atmospheric vapor pressure deficit reduces global vegetation growth. *Sci. Adv.* **5**, eaax1396 (2019).
31. Peters, W., Luijckx, I., Loubet, B. & Loustau, D. Temperature extremes of 2022 reduced carbon uptake by forests in Europe. *Nat. Commun.* **14**, 1–11 (2023).
32. Frank, D. et al. Effects of climate extremes on the terrestrial carbon cycle: Concepts, processes and potential future impacts. *Glob. Chang Biol.* **21**, 2861–2880 (2015).
33. Zhang, Y. et al. Increasing sensitivity of dryland vegetation greenness to precipitation due to rising atmospheric CO₂. *Nat. Commun.* **13**, 4875 (2022).
34. Corak, N. K., Otkin, J. A., Ford, T. W. & Lowman, L. E. L. Unraveling phenological and stomatal responses to flash drought and implications for water and carbon budgets. *Hydrol. Earth Syst. Sci.* **28**, 1827–1851 (2024).
35. Liu, L., Gudmundsson, L. & Seneviratne, S. I. Soil moisture dominates dryness stress on ecosystem production globally. *Nat. Commun.* **11**, 4892 (2020).
36. Li, F. et al. Global Water Use Efficiency Saturation Due to Increased Vapor Pressure Deficit. *Science* **381**, 672–677 (2023).
37. Peters, W. et al. Increased water-use efficiency and reduced CO₂ uptake by plants during droughts at a continental scale. *Nat. Geosci.* **11**, 744–748 (2018).
38. Yang, Y. et al. Contrasting responses of water use efficiency to drought across global terrestrial ecosystems. *Sci. Rep.* **6**, 23284 (2016).
39. Smith, T., Traxl, D. & Boers, N. Empirical evidence for recent global shifts in vegetation resilience. *Nat. Clim. Chang* **12**, 477–484 (2022).
40. Forzieri, G., Dakos, V., McDowell, N. G., Ramdane, A. & Cescatti, A. Emerging signals of declining forest resilience under climate change. *Nature* **608**, 534–539 (2022).
41. Green, J. K., Berry, J., Ciais, P., Zhang, Y. & Gentine, P. Amazon rainforest photosynthesis increases in response to atmospheric dryness. *Sci. Adv.* **6**, eabb7232 (2020).
42. Feng, X. et al. Recent leveling off of vegetation greenness and primary production reveals the increasing soil water limitations on the greening Earth. *Sci. Bull.* **66**, 1462–1471 (2021).
43. Breiman, L. Random Forests. *Mach. Learn* **45**, 5–32 (2001).
44. Zhu, Z. et al. Greening of the Earth and its drivers. *Nat. Clim. Chang* **6**, 791–795 (2016).
45. Piao, S. et al. Characteristics, drivers and feedbacks of global greening. *Nat. Rev. Earth Environ.* **1**, 14–27 (2020).
46. Zhang, Y., Keenan, T. F. & Zhou, S. Exacerbated drought impacts on global ecosystems due to structural overshoot. *Nat. Ecol. Evol.* **5**, 1490–1498 (2021).
47. Zhang, M., Yuan, X., Otkin, J. A. & Ji, P. Climate warming outweighs vegetation greening in intensifying flash droughts over China. *Environ. Res. Lett.* **17**, 054041 (2022).
48. Ciais, P. et al. Europe-wide reduction in primary productivity caused by the heat and drought in 2003. *Nature* **437**, 529–533 (2005).
49. Ullah, I. et al. Anthropogenic and atmospheric variability intensifies flash drought episodes in South Asia. *Commun. Earth Environ.* **5**, 267 (2024).
50. Anderegg, W. R. L. et al. Pervasive drought legacies in forest ecosystems and their implications for carbon cycle models. *Science* **349**, 528–532 (2015).
51. Yin, J. et al. Future socio-ecosystem productivity threatened by compound drought–heatwave events. *Nat. Sustain* **6**, 259–272 (2023).
52. Lesk, C., Rowhani, P. & Ramankutty, N. Influence of extreme weather disasters on global crop production. *Nature* **529**, 84–87 (2016).
53. Lobell, D. B. et al. Greater sensitivity to drought accompanies maize yield increase in the U.S. Midwest. *Science* **344**, 516–519 (2014).
54. Hunt, E. et al. Agricultural and food security impacts from the 2010 Russia flash drought. *Weather Clim. Extrem* **34**, 100383 (2021).
55. Jain, P. et al. Drivers and Impacts of the Record-Breaking 2023 Wildfire Season in Canada. *Nat. Commun.* **15**, 6764 (2024).
56. Hersbach, H. et al. The ERA5 global reanalysis. *Q. J. R. Meteorological Soc.* **146**, 1999–2049 (2020).
57. Cosgrove, B. et al. The Global Land Data Assimilation System. *Bull. Am. Meteorol. Soc.* **85**, 381–394 (2004).
58. Martens, B. et al. GLEAM v3: Satellite-based land evaporation and root-zone soil moisture. *Geosci. Model Dev.* **10**, 1903–1925 (2017).
59. Samaniego, L., Kumar, R. & Zink, M. Implications of parameter uncertainty on soil moisture drought analysis in Germany. *J. Hydrometeorol.* **14**, 47–68 (2013).
60. Samaniego, L. et al. Propagation of forcing and model uncertainties on to hydrological drought characteristics in a multi-model century-long experiment in large river basins. *Clim. Change* **141**, 435–449 (2017).
61. Zhou, S., Bofu, Y., Huang, Y. & Wang, G. Daily underlying water use efficiency for AmeriFlux sites. *J. Geophys Res Biogeosci.* **120**, 887–902 (2015).
62. Huang, J., Yu, H., Guan, X., Wang, G. & Guo, R. Accelerated dryland expansion under climate change. *Nat. Clim. Chang* **6**, 166–171 (2016).
63. Running, S. W. et al. A Continuous Satellite-Derived Measure of Global Terrestrial Primary Production. *Bioscience* **54**, 547–560 (2004).
64. Sun, Y. et al. OCO-2 advances photosynthesis observation from space via solar-induced chlorophyll fluorescence. *Science* **358**, eaam5747 (2017).
65. Li, X. et al. Solar-induced chlorophyll fluorescence is strongly correlated with terrestrial photosynthesis for a wide variety of biomes: First global analysis based on OCO-2 and flux tower observations. *Glob. Chang Biol.* **24**, 3990–4008 (2018).
66. Wang, X., Qiu, B., Li, W. & Zhang, Q. Impacts of drought and heat-wave on the terrestrial ecosystem in China as revealed by satellite solar-induced chlorophyll fluorescence. *Sci. Total Environ.* **693**, 133627 (2019).
67. Li, X. & Xiao, J. A Global, 0.05-Degree Product of Solar-Induced Chlorophyll Fluorescence Derived from OCO-2, MODIS, and Reanalysis Data. *Remote Sens* **11**, 517 (2019).
68. Rakovec, O. et al. The 2018–2020 Multi-Year Drought Sets a New Benchmark in Europe. *Earths Fut.* **10**, e2021EF002394 (2022).
69. Otkin, J. A. et al. Development of a flash drought intensity index. *Atmosphere* **12**, 741 (2021).
70. Zhang, Y., Parazoo, N. C., Williams, A. P., Zhou, S. & Gentine, P. Large and projected strengthening moisture limitation on end-of-season photosynthesis. *Proc. Natl Acad. Sci.* **117**, 9216–9222 (2020).

71. Davison, A. & Hinkley, D. *Bootstrap Methods and Their Application* (Cambridge University Press, Cambridge, 1997).

Acknowledgements

This work was supported by the National Natural Science Foundation of China (42205030, 42330604), National Key Research and Development Program of China (2022YFC3002803). PW was funded by the Met Office Climate Science for Service Partnership (CSSP) China project under the International Science Partnerships Fund (ISPF). J.X. was supported by the Iola Hubbard Climate Change Endowment managed by the Earth Systems Research Center at the University of New Hampshire. T.F.K. acknowledges support from a DOE Early Career Research Program award #DE-SC0021023 and NASA Awards 80NSSC21K1705, 80NSSC20K1801 and 80NSSC25K7327. We acknowledge the high-performance computing support from the National Key Scientific and Technological Infrastructure project “Earth System Numerical Simulation Facility” (EarthLab).

Author contributions

M.Z. and X.Y. conceived this study and designed the methodology. M.Z. processed the data and performed the analysis. J.X. developed the GOSIF dataset. M.Z. wrote the original draft with suggestions from X.Y., Z.Z.Z., M.P., P.L.W., and T.F.K. All authors interpreted results and edited the manuscript.

Competing interests

The authors declare no competing interests.

Additional information

Supplementary information The online version contains supplementary material available at <https://doi.org/10.1038/s41467-025-58253-z>.

Correspondence and requests for materials should be addressed to Xing Yuan.

Peer review information *Nature Communications* thanks Luis Samaniego and the other, anonymous, reviewer(s) for their contribution to the peer review of this work. A peer review file is available.

Reprints and permissions information is available at <http://www.nature.com/reprints>

Publisher's note Springer Nature remains neutral with regard to jurisdictional claims in published maps and institutional affiliations.

Open Access This article is licensed under a Creative Commons Attribution-NonCommercial-NoDerivatives 4.0 International License, which permits any non-commercial use, sharing, distribution and reproduction in any medium or format, as long as you give appropriate credit to the original author(s) and the source, provide a link to the Creative Commons licence, and indicate if you modified the licensed material. You do not have permission under this licence to share adapted material derived from this article or parts of it. The images or other third party material in this article are included in the article's Creative Commons licence, unless indicated otherwise in a credit line to the material. If material is not included in the article's Creative Commons licence and your intended use is not permitted by statutory regulation or exceeds the permitted use, you will need to obtain permission directly from the copyright holder. To view a copy of this licence, visit <http://creativecommons.org/licenses/by-nc-nd/4.0/>.

© The Author(s) 2025